A 3D GENERALIZED RIGID PARTICLE
CONTACT MODEL FOR ROCK FRACTURE
N. MONTEIRO AZEVEDO[*], J. LEMOS[*]

[*] Concrete Dams Department
Laboratório Nacional de Engenharia Civil (LNEC)
Av. Do Brasil 101, 1700-066 Lisboa Portugal
e-mail: {nazevedo, vlemos} @lnec.pt, www.lnec.pt/organizacao/dbb

Key words: DEM, Contact model, Fracture, Rock.

Abstract. Detailed rigid particle models have been proposed for modeling fracture in quasi-brittle materials. The rigid particle circular models proposed in the literature do not properly reproduce the known rock friction angle and the observed rock tensile strength to compression strength ratio. In this article, a 3D rigid particle contact model, 3D-GCM, is presented which has been developed to study fracture phenomena in rock. The 3D-GCM contact model incorporates in a straightforward manner the force versus displacement relationships of the traditional contact point contact model model, PCM. Furthermore it provides both moment transmission and simple physical constitutive models based on standard force displacement relationships. The 3D-GCM model is validated against known triaxial and Brazilian tests of a granite rock. It is shown that the enhanced rigid particle model leads to a better agreement with the experimental results.

1 INTRODUCTION

Detailed rigid particle models have been introduced in the study of fracture of continuous media such as concrete and rock in the early 1990's [1-6]. More recently 3D rigid spherical particle models have been proposed for rock, [7, 8], and for concrete, [9-11]. Models based on the rigid spring block method adopting 3D Voronoi shape polyhedra have also been developed for concrete, [12-13].

Through the simulation of the material meso-structure, the rigid particle models prevent localization of damage into regions not sufficiently large when compared to the inhomogeneity size. Particle models are conceptually simpler than a continuum approach, and the development of cracks and rupture surfaces appears naturally as part of the simulation process given its discrete nature. As discussed in Cundall [14], assemblies of discrete particles connected through simple interaction laws are able to capture the global behaviour of quasi-brittle macro-material, like concrete or rock. The parameters of the interaction laws may require some calibration at the micro-level.

In rock fracture studies the bonded particle model, BPM, [8] has received considerable attention given its known ability to model rock complex behaviour, namely in uniaxial compression. It adopts the traditional single point contact model, PCM, for grain behaviour, in parallel with a contact model that allows moment transmission through a rotational

stiffness spring, parallel bond, PB, which attempts to simulate the cement behaviour. The BPM model, as presented in [8], is not able to model the ratio of tensile strength to compressive strength that occurs in rock. Also the macroscopic friction angle obtained through triaxial testing is quite low when compared to the known rock experimental values.

In this work, a 3D generalized contact model, 3D-GCM, based on the 2D contact model [15] is presented. The number of local points used in the contact discretization is a model parameter and can be set to a given value. With the 3D-GCM it is still possible to model the traditional PCM contact model adopting only one contact point. By increasing the density of local contact points the elastic response converges to the response obtained with the PB contact model which adopts a uniform distribution of local points [8].

The proposed model is validated against known triaxial and Brazilian tests in a granite rock. It is shown that the enhanced rigid particle model leads to a better agreement with the known experimental results.

2 FORMULATION

2.1 Fundamentals

In the DEM, the domain is replaced by an assembly of discrete entities that interact with each other through contact points or contact interfaces. The ability to include finite displacements and rotations, including complete detachment, and to recognize new contacts as the calculation progresses are essential features. The set of forces acting on each particle are related to the relative displacements of the particle with respect to its neighbours. At each step, given the applied forces, Newton's 2nd law of motion is invoked to obtain the new position of the particle. The equations of motion, including local non-viscous damping, of a particle may be expressed as:

$$
\begin{aligned}
F_i(t) + F_i^{\,d}(t) &= m\,\ddot{x}_i + m\,\dot{x}_i \\
M_i(t) + M_i^{\,d}(t) &= I\,\dot{\omega}_i + I\,\omega_i
\end{aligned}
\tag{1}
$$

where: $F_i(t)$ and $M_i(t)$ are, respectively, the total applied force and moment at time t including the exterior contact contribution, m and I are, respectively, the particle mass and moment of inertia, $\ddot{x}_i$ and $\dot{x}_i$ are the particle acceleration and velocity, $\dot{\omega}_i$ and ω_i are, respectively, the particle angular acceleration and velocity. The damping forces are given by:

$$
\begin{aligned}
F_i^{\,d}(t) &= -\alpha\,|F_i(t)|\,sign(\dot{x}_i) \\
M_i^{\,d}(t) &= -\alpha\,|M_i(t)|\,sign(\omega_3)
\end{aligned}
\tag{2}
$$

being, $\dot{x}_i$ the particle velocity and α the local non-viscous damping and the function sign (x) given by:

$$
sign(x) = \begin{cases} +1\,, & x > 0 \\ -1\,, & x < 0 \\ 0\,, & x = 0 \end{cases}
\tag{3}
$$

2.2 Generalized contact model (3D-GCM)

The 3D-GCM as defined is based on the 2D-GCM contact model that considers on a given contact width a discrete number of local contact points that are able to transfer normal and shear forces [15]. In the 3D-GCM contact model, one can have on an idealized cylindrical contact surface, several concentric circular clouds of contact points, Figure 1.
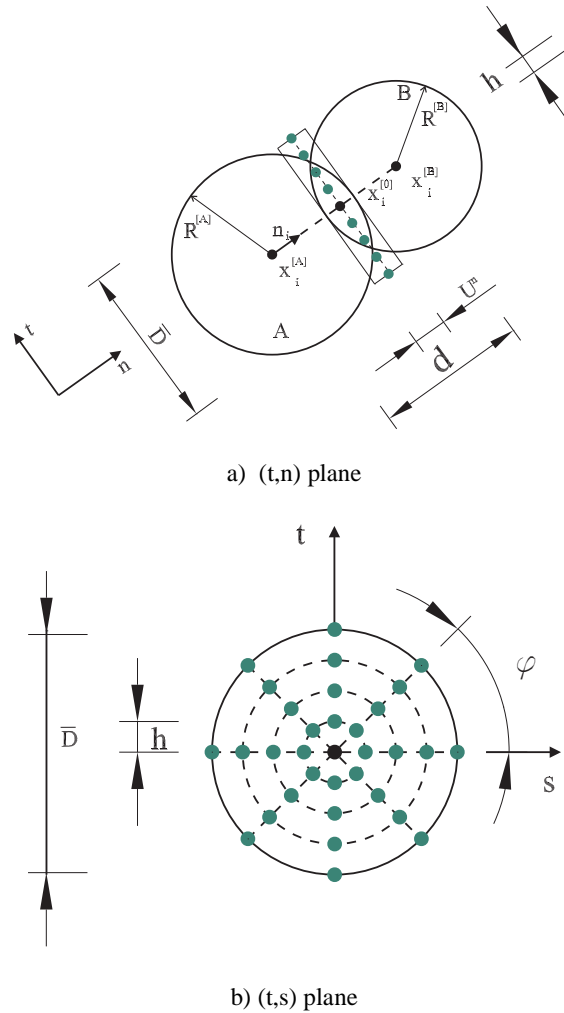

a) (t,n) plane

b) (t,s) plane

Figure 1: 3D-GCM contact model discretizations

The number of layers and the total number of points per layer is a model parameter. As the number of contacts points is increased, one obviously obtains the equivalent continuum solution, PB contact model [8]. Given the contact surface discretization, it is possible to

transfer through the contact surface both force, bending and torsional moments. As referred, the traditional PCM contact model only allows the transmission of force. The contact unit normal is defined given the particles centre of gravity and the inter-particle distance, see Figure 1a):

$$n_i = \frac{x_i^{[B]} - x_i^{[A]}}{d} \tag{4}$$

The contact overlap for the reference contact point and its location are given by:

$$
\begin{aligned}
U^n &= R^{[A]} + R^{[B]} - d \\
x_i^{[0]} &= x_i^{[A]} + \left(R^{[A]} - \frac{1}{2} U^n \right) n_i
\end{aligned}
\tag{5}
$$

In the 3D-GCM contact model it is further required to set for each local contact point, its contact location and local contact overlap. For this reason, a local *(t,s)* axys is defined, Figure 1b). Given the contact discretization one needs to know for each local contact point, its local coordinates relative to the reference contact point. Then the local contact point position in global coordinates can be defined using:

$$x_i^{[j]} = x_i^{[0]} + s^{[j]} x_i^{[s]} + t^{[j]} x_i^{[t]} \tag{6}$$

where: $x_i^{[s]}$ and $x_i^{[t]}$ are the global coordinates of the local *s* axys and local *t* axys, respectively. The contact forces that are acting on each local contact point can be decomposed into its normal and shear component with respect to the contact plane:

$$F_i^{[J]} = F_i^{[n,J]} + F_i^{[s,J]} \tag{7}$$

The contact velocity of a given local contact point, which is the velocity of particle B relative to particle A, at the contact location is given by:

$$
\begin{aligned}
\dot{x}_i^J &= \left(\dot{x}_i^J \right)_B - \left(\dot{x}_i^J \right)_A \\
&= \left(\dot{x}_i^B + \varepsilon_{ijk} \omega_j^B \left(\dot{x}_i^J - \dot{x}_i^B \right) \right) - \left(\dot{x}_i^{A_1} + \varepsilon_{ijk} \omega_j^A \left(\dot{x}_i^J - \dot{x}_i^A \right) \right)
\end{aligned}
\tag{8}
$$

The contact displacement normal increment, $\Delta x^{J,N}$, stored as a scalar, and shear increment, $\Delta x_i^{J,S}$, stored as a vector, are given by:

$$
\begin{aligned}
\Delta x^{J,N} &= \left(\dot{x}_i^J \Delta t \right) n_i \\
\Delta x_i^{J,S} &= \left(\dot{x}_i^J \Delta t \right) - \Delta x^{J,N} n_{i\,i}
\end{aligned}
\tag{9}
$$

The local contact point overlap is defined incrementally for all the local points based on the current contact velocity time step, Δt:

$$U^{J,n} = U^{J,n.old} + \left(\dot{x}_i^J \ n_i \right) \Delta t \tag{10}$$

Given the normal and shear stiffness of the local contact point, the normal and shear forces increments are obtained following an incremental linear law:

$$
\begin{aligned}
\Delta F^{J,N} &= -k_n \ \Delta x^{J,N} \\
\Delta F_i^{J,S} &= -k_s \ \Delta x_i^{J,S}
\end{aligned}
\tag{11}
$$

The predicted normal and shear forces acting at the local contact point are then updated by applying the following equations:

$$
\begin{aligned}
F^{J,N.new} &= F^{J,N.old} + \Delta F^{J,N} \\
F_i^{J,S.new} &= F_i^{J,S.old} - \varepsilon_{ijk}\varepsilon_{kmn} F_k^{J,S.old} n_m^{old} n_n + \Delta F_i^{J,S}
\end{aligned}
\tag{12}
$$

Due to the fact that the shear contact force is stored in global coordinates, it is necessary to redefine it in the updated contact plane. Given the predictive normal and shear contact forces, the adopted constitutive model is applied. If the predictive forces do not satisfy the constitutive model an adjustment, that is model dependent, needs to be carried. The resultant contact force at the local contact point is then given by:

$$F^J = F^{J,N} \ n_i + F_i^{J,S} \tag{13}$$

At the reference contact point, the resultant contact force and contact moment are defined given the contribution from all the contact points:

$$
\begin{aligned}
F_i^{[C]} &= \sum_J F_i^J \\
M_i^{[C]} &= -\sum_J \varepsilon_{ijk}\left(x_j^J - x_j^0 \right)F_k^J
\end{aligned}
\tag{14}
$$

The contact force and moment are then transferred to the particle centre of gravity of each particle in contact through:

$$
\begin{aligned}
F_i^{[A]} &= F_i^{[A]} - F_i^{[C]} \\
F_i^{[B]} &= F_i^{[B]} + F_i^{[C]}
\end{aligned}
\tag{15}
$$

$$
\begin{aligned}
M_i^{[A]} &= M_i^{[A]} - \varepsilon_{ijk}\left(x_j^0 - x_j^A \right)F_k^{[C]} - M_i^{[C]} \\
M_i^{[B]} &= M_i^{[B]} + \varepsilon_{ijk}\left(x_j^0 - x_j^B \right)F_k^{[C]} + M_i^{[C]}
\end{aligned}
\tag{16}
$$

5

2.3 Numerical stability

When only a steady state solution is sought, a mass scaling algorithm is adopted in order to reduce the number of time steps necessary to reach the desired solution. The particle mass and inertia are artificially scaled so the centred-difference algorithm has a higher rate of convergence for a given loading step. The particle scaled mass and inertia, used in the calculations are set assuming a unit time increment, given the particle stiffness at a given time through:

$$m^{scaled} = 0.25\ k_t\ ;\ I^{scaled} = 0.25\ k_\theta \tag{17}$$

The total translation stiffness k_t and the rotational stiffness k_θ of each particle must include the contribution of all particles in contact at a given time step:

$$
\begin{aligned}
k_t &= \sum_{c=1}^{N} 2\left(\sum_j k_n^J + \sum_j k_s^J \right) \\
k_\theta &= \sum_{c=1}^{N} \left(K_s d_{AC}^2 + K_s d_{AC} d_{BC} + 2K_s R^2 + 2K_n R^2 \right)
\end{aligned}
\tag{18}
$$

where: $K_s = \sum_j k_s^J$, $K_s R^2 = \sum_j k_s^J \left(\left(s^J\right)^2 + \left(t^J\right)^2 \right)$ and $K_n R^2 = \sum_j k_n^J \left(\left(s^J\right)^2 + \left(t^J\right)^2 \right)$.

2.4 Local contact stiffness and local contact strength

In this work the total 3D-GCM contact stiffness associated to the contact is given by:

$$
\begin{aligned}
K_n &= \overline{E}\ \frac{\pi \overline{R}^2}{d} \\
K_s &= \eta\ K_n
\end{aligned}
\tag{19}
$$

where: $\overline{R}$ is minimum radius of the particles in contact, d is the distance between the particles in contact, $\overline{E}$ is the Young modulus of the equivalent continuum material and η is a constant that relates the normal and the shear stiffness spring value. The total tensile and shear contact strength are defined given the maximum stresses and the contact area by:

$$
\begin{aligned}
F_{n.t} &= \overline{\sigma}_{n.t} \pi \overline{R}^2 \\
F_s &= \overline{\tau}\ \pi \overline{R}^2
\end{aligned}
\tag{2}
$$

The contact properties, strength and stiffness of each local contact point are then defined given the contact local weight and the total contact values. In this work the same weight is given to the local points. For the local inter-particle contacts, a brittle Mohr-Coulomb model including a frictional term before failure with tension cut-off is adopted, Figure 2. As soon as

the maximum shear or tensile strength is reached the local contact is considered to be cracked only transferring forces under compression.
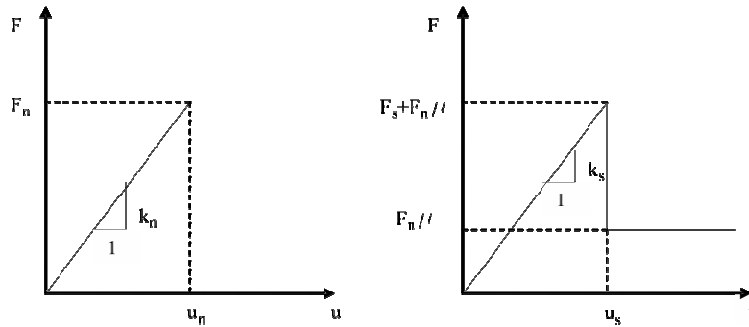

Figure 2: 3D-GCM local contact constitutive model

2.5 Particle generation scheme

The particle assemblies here presented have been generated using the algorithms proposed in [8]. The initial circular particle assembly is created by first inserting the particles with half their radius guaranteeing that the particles do not overlap with each other, Figure 3a). Then the particle real radius is adopted, and a DEM cohesionless type solution is obtained, leading to a redistribution of the particle overlap throughout the assembly. The final assembly, Figure 3b), is obtained by setting the desired initial isotropic stress, followed by a floater elimination procedure, [8].
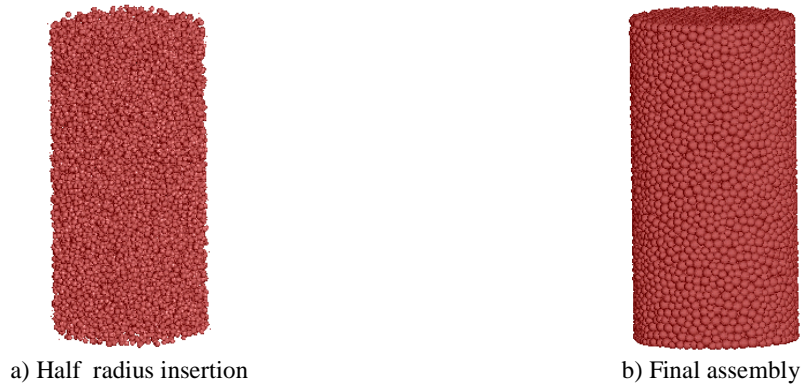

a) Half radius insertion   b) Final assembly

Figure 3: Particle assembly for a granite rock

The particle assemblies generated, similar to the presented in [8], are then triangulated using a Delaunay scheme. In this work it is considered that two particles interact with a GCM contact model if they share a common Delaunay tetrahedron edge, even if they are not in real contact. When compared to the particle assemblies presented in [8], where only particles closer than 1×10^{-6} of the average radius are considered to be in contact, the number of connections is significantly increased.

3   TRIAXIAL AND BRAZILIAN TEST IN A GRANITE ROCK

The 3D-GCM model is validated against triaxial and Brazilian tests in a granite rock (Lac du Bonet) [8]. The tests were performed in cylindrical specimens with a 0.0634 m height and 0.0317 m radius. Two different particles assembly sizes were adopted. A coarser assembly with a uniform diameter distribution ranging from 1.50 mm to 2.49 mm, with a total average of 7800 particles. And a finer particle assembly, with a uniform diameter distribution ranging from 1.19 mm to 1.98 mm, with 15600 particles in average.

In the triaxial tests the initial isotropic pressure is applied through the vertical and lateral confinement walls, Figure 4a). After setting the isotropic stress, a small downward velocity is given to the upper vertical wall, 0.25×10^{-8} m/s, in order to simulate quasi-static conditions. The lateral walls are subdivided into several polyhedrical pieces that do not interact with each other and can only have inward displacement, in order to approximate the behaviour of a flexible membrane. Also with this purpose, the lateral wall contacts with the spherical particles have a lower stiffness, around 10% of the inter-particle stiffness. In the Brazilian tests the quasi-static load is applied by giving a downward velocity, 0.75×10^{-9} m/s, to the upper plate.

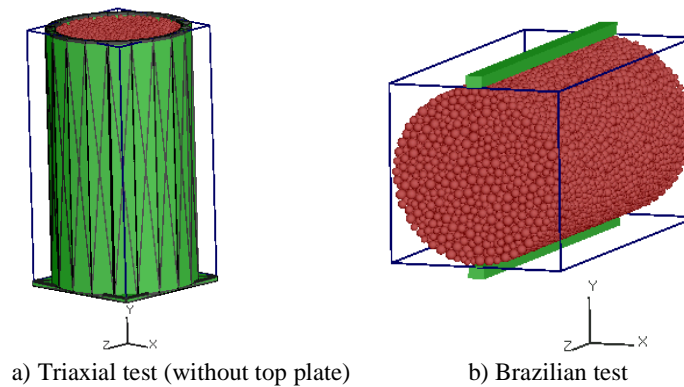a) Triaxial test (without top plate)   b) Brazilian test

Figure 4: Particle assemblies – Boundary conditions

Table 1 presents the micromechanical elastic and strength properties that were adopted for the different particle assemblies adopted. Given some difficulties in matching the Poisson ratio of the Lac du Bonet granite ($\nu = 0.26$) it was also assessed a GCM model with different spring stiffness for tensile and compression loading. For the GCM contact a local discretization of 5 local points was adopted, one central point and four peripherical local points, all with the same local weight. The strength micro-parameters were calibrated on a trial and error basis in order to match the experimental uniaxial compression strength and the Brazilian test tensile strength.

Table 1: Micro-properties for Lac du Bonet granite

	K_n (tension)	K_n (compression)	η	$\bar{\sigma}_{n,t}$ [MPa]	$\bar{\tau}$ [MPa]	μ
GCM-A1	50.0	-	0.25	33.5	43.5	0.30
GCM-A2	24.0	48.0	0.30	25.0	33.0	0.30
GCM-B1	50.0	-	0.25	33.0	44.0	0.30
GCM-B1	24.0	48.0	0.30	25.0	33.5	0.30

Table 2 presents the macro strength properties obtained with the different particles assemblies and contact models. It can be identified that a spring with reduced value under tensile loading increases the Poisson ratio. In order to match the Poisson ratio with a constant spring stiffness it would be necessary to adopt a constant $\eta = \dfrac{K_n}{K_s}$ lower than 0.07, which can be considered to be quite low. In [8] a similar mechanism was adopted, the cemented contacts, PB type, work under compression in parallel with granular type contacts, and under tensile loading only the PB contacts carry the tensile loading.

The macroscopic friction angle and the cohesion values are set according to the expressions defined in [8] that take as input the triaxial results. Lac du Bonet granite is considered to have an average friction angle of 59º and a cohesion value of 30 MPa [8]. The numerical macroscopic friction angle is still lower than the Lac du Bonet value, $\phi = 59.0º$, but it is in much better agreement when compared with the numerical value obtained in [8] ($\phi = 32.1º$) with an equivalent spherical model and particle assembly. The uniaxial maximum compression values are also in good agreement with the Lac du Bonet granite that has a known average value of 200.0 MPa.

Table 2: Macro-properties for Lac du Bonet granite

	E [GPa]	ν	q_u [MPa]	ϕ [º]	C [MPa]	σ_t [MPa]	q_u/σ_t
GCM-A1	72.8	0.19	202.1	44	42.5	28.7	7.0
GCM-A2	72.7	0.24	201.6	40	47.5	28.5	7.1
GCM-B1	74.0	0.18	205.5	46	41.6	26.4	7.8
GCM-B1	73.5	0.23	203.3	43	43.9	24.3	8.4

Table 2 also shows that the 3D-GCM contact model with a brittle contact law is not able to model the ratio of compression strength to tensile strength. The Lac du Bonet granite has a known 21.5 ratio. This shows that the 3D-GCM contact model needs to be further enhanced, for example by considering the fracture energy at the micro-level.
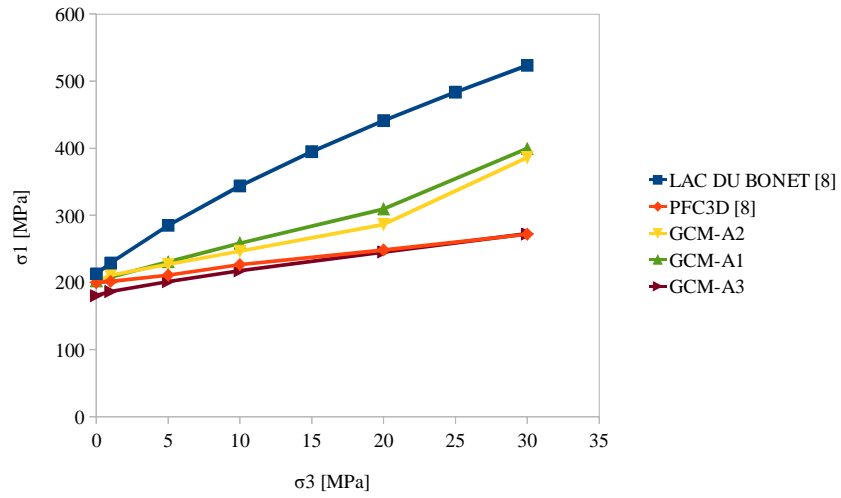
a) Coarse assembly A
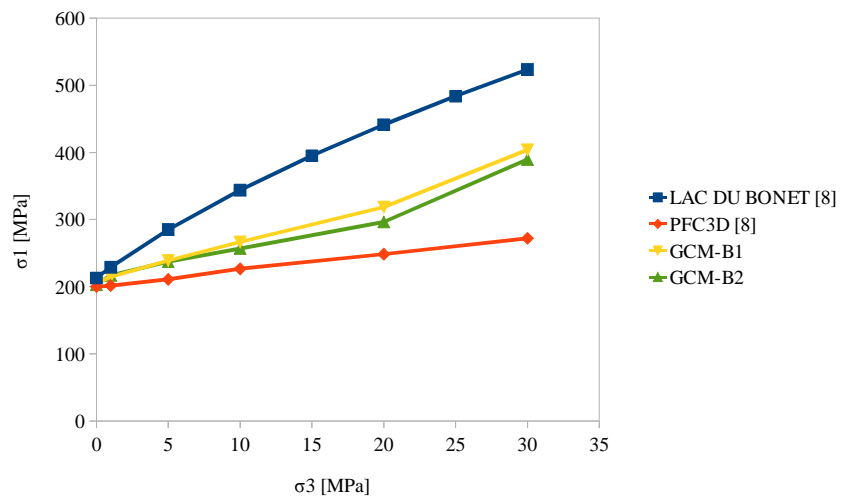
b) Finer assembly B

Figure 5 : Strength envelope for the 3D-GCM models and experimental testing [8]

Figure 5 compares the strength envelope results obtained with the 3D-GCM contact model with an equivalent spherical particle model [8] and with the experimental results obtained for Lac du Bonet granite [8]. It can be seen that the 3D-GCM contact model leads to a better agreement with the known Lac du Bonet strength envelope.

Figure 5a) presents the strength envelope obtained with a zero micro-mechanical

friction angle, $\mu = 0.0$, GCM-A3. Note that the latter strength envelope is close to the obtained with an equivalent spherical model that also does not include the friction angle at the inter-particle contact [8]. This shows that the friction angle value, that can be straightforwardly included within a GCM-contact formulation, is relevant in order to have a better agreement with the known experimental value.

12 CONCLUSIONS

A generalized 3D contact model, 3D-GCM, is presented which is defined through identifiable mechanisms of shear and normal force transfer through the contact interface. In this paper, the GCM contact model is adopted in the interaction between particles that share a common tetrahedron edge. Note that when compared to other particle models for rock [8] each particle has a higher number of particle interactions.

The 3D-GCM contact model incorporates in a straightforward manner the force versus displacement relationships of the traditional contact point contact model model, PCM, providing both moment transmission and simple physical constitutive models based on standard force displacement relationships. The results indicate that 4 local points at the outer boundary of the contact are sufficient in order to obtain complex macro-responses.

It is also shown that 3D-GCM model between spherical particles by incorporating a frictional term at the inter-particle contact level leads to a more realistic hard rock macroscopic behaviour, namely the macroscopic friction angle is increased.

Finally, the 3D-GCM contact model with a brittle contact law is not able to model the ratio of compression strength to tensile strength of the Lac du Bonet granite. It is expectable to have a better agreement with the real response if a more complex contact constitutive law, e.g. softening at the contact level, is incorporated within a 3D-GCM contact model.

REFERENCES

[1] Zienkiewicz, O.C. and Taylor, R.L. The finite element method. McGraw Hill, Vol. I., (1989), Vol. II, (1991).

[2] Bolander, J.E. and Saito, S. Fracture analyses using spring networks with random geometry. *Engineering Fracture Mechanics* (1998) **61 (8)**:569-591.

[3] Meguro, K. and Hakuno, M. Fracture analysis of concrete structures by the modified distinct element method. *Structural Engineering / Earthquake Engineering* (1989) **6(2)**:283-294.

[4] Potyondy, D. and Cundal, P.A. Modeling rock using bonded assemblies of circular particles, Aubertin, Hassani, Mitri eds. 2nd North American Rock Mechanics

Symposium,. Balkema (1996), 1937-1944.

[5] Schlangen, E. and Garboczi, E. Fracture simulations of concrete using lattice models: Computational aspects. *Engineering Fracture Mechanics* (1997) **57 (2/3)**:319-332.

[6] S. Takada, N. Hassani, Analysis of compression failure of reinforced concrete by the modified distinct element method. Manolis B, Beskos DE eds. Advances in earthquake engineering, earthquake resistant engineering structures. Computational Mechanics Publications, (1996).

[7] Matsuda Y. and Iwase, Y. Numerical simulation of rock fracture using three-dimensional extended discrete element method. *Earth Planets Space* (2002) **54**: 367-378.

[8] Potyondy, D. and Cundall, P.A. A bonded-particle model for rock. *Int J Rock Mech Min Sci* (2004) **41**:1329-1364.

[9] Cusatis, P., Bazant, Z. and Cedolin, L. Confinement-shear lattice CSL model for fracture propagation in concrete. *Computer Methods in Applied Mechanics and Engineering* (2006) **195 (52-1)**:7154-7171.

[10]   Hentz, S., Daudeville, L. and Donze, V. Identification and Validation of a discrete element model for concrete. *Journal of Engineering Mechanics ASCE* (2004) **130(6)**:709-719.

[11]   Lilliu, J.G. and Van Mier, M. 3D lattice type fracture model for concrete. *Engineering Fracture Mechanics*, (2003) **70 (7-8):**841-927.

[12]   Berton, S. and Bolander, J.E. Crack band model of fracture in irregular lattices. *Computer Methods in Applied Mechanics and Engineering* (2006) **195(52)**:7172-7181.

[13]   Nagai, K., Sato, Y. and Ueda, T. Mesoscopic simulation of failure of mortar and concrete by 3D RBSM. *Journal of Advanced Concrete Technology* (2005) **3(3)**:385-402.

[14]   Cundall, P. A discontinuous future for numerical modelling in geomechanics?. *Geotechnical Engineering* (2001) **149(1)**:41-47.

[15]   Monteiro-Azevedo, N. and Lemos, J.V. A generalized rigid particle contact model for fracture analysis. *International Journal for Numerical and Analytical Methods in Geomechanics* (2005) **29**:269-285.